



Nanodisperse gold catalysts in oxidation of benzyl alcohol: comparison of various supports under different conditions

Gergely Nagy, et al. [full author details at the end of the article]

Received: 15 April 2019 / Accepted: 2 June 2019 / Published online: 21 June 2019
© The Author(s) 2019

Abstract

Monodisperse gold particles (ca. 2 nm) were prepared and deposited on various supports (SiO_2 , Al_2O_3 , HAP, MgAl_2O_4 and MgO). The acid/base properties of supports were characterized by NH_3 and CO_2 sorption. The size of the gold nanoparticles spans in the 1.7–6.5 nm mean diameter range after calcination as determined from TEM measurements. The amounts of accessible surface sites were estimated by binary concentration pulse chromatography of CO with Kr adsorption. The data are in agreement with the results of CO adsorption obtained by DRIFT spectroscopy. The activities of the catalysts were compared in the oxidation of benzyl alcohol in stirred batch reactors under two different conditions: in xylene solvent with atmospheric oxygen at 60 °C (in presence and in absence of K_2CO_3), and in a solvent-free mixture at elevated pressure and temperature (5 bar O_2 , 150 °C, 5 h). The activities of catalysts in benzyl alcohol conversion are described in two variants, namely related to (i) active catalytic sites (ASNA), and (ii) number of Au atoms on the geometric surface of particles (GSNA). The activities of catalysts in xylene solvent at 60 °C were excellent, with 0.28–1.11 s^{-1} characteristic GSNA_{ini} values (initial reaction rates related to surface Au atoms, Au_{surf}) in presence of K_2CO_3 . The observed order of activities under these conditions is $\text{Au/SiO}_2 < \text{Au/Al}_2\text{O}_3 < \text{Au/HAP} < \text{Au/MgAl}_2\text{O}_4 < \text{Au/MgO}$. In the experiments performed at 150 °C under solvent-free conditions, the reaction partners are depleted in greater extents (with the exception of $\text{Au/Al}_2\text{O}_3$), thus the obtained average GSNA_{ave} (average reaction rate during 5 h reaction related to Au_{surf}) values are less reliable, however selectivity data provide useful information as well. These estimated average GSNA_{ave} values (0.14–0.83 s^{-1}) attest still good activities. For the interpretation of the obtained data, the roles of active sites on gold nanoparticles of various dispersion and the accessibility of their surfaces as well as the acid–base properties and surface hydroxyl concentration of supports, water ad- and desorption phenomena are considered simultaneously.

Electronic supplementary material The online version of this article (<https://doi.org/10.1007/s11144-019-01615-8>) contains supplementary material, which is available to authorized users.

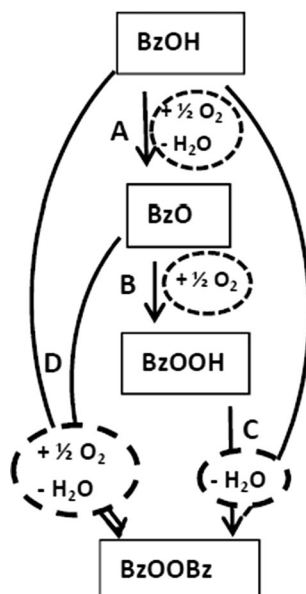
Keywords Benzyl alcohol oxidation · Supported gold catalysts · Distinction of active sites · Acid/base support effects · Binary concentration pulse chromatography

Introduction

Among wide catalytic applications of supported gold nanoparticles [1, 2], oxidation of benzyl alcohol (BzOH) to benzaldehyde (BzO) or to benzoic acid (BzOOH) had also been in the focus of several studies. The reaction can be performed directly, by mixing the catalyst and the alcohol in the presence of oxygen, or in a reaction medium by using a solvent, which can either be an organic one, or water, and mixed, organic-aqueous media is applied often as well [3–5]. Furthermore, the addition of inorganic bases (NaOH, K_2CO_3 , etc.) may significantly hinder the deactivation of catalyst [6, 7] and favours the formation of intermediate alcoholate [8]. In addition, it influences the selectivity and, in aqueous solution and under solvent-free conditions, promotes the formation of benzoic acid, in organic media benzyl benzoate (BzOOBz) [4, 7]. The dehydrogenation of alcohols to aldehydes can also be performed under anaerobic conditions with similar supported gold catalysts [9]. The absence or presence and the participation of water is also crucial, it may contribute in different extents to the various elementary steps of the set of processes in the oxidation of BzOH [4, 5, 7, 10].

The conversion of BzOH by oxidation may take place in various reactions (A–D, Scheme 1). First, the alcohol, BzOH, can be oxidized to aldehyde, BzO (reaction A). The oxidation of BzO may proceed further in two directions. Namely, BzO may be converted to benzoic acid, BzOOH in reaction B and in a further step BzOOBz ester can be formed from BzOOH and from the starting BzOH (reaction C). In another

Scheme 1 Various reaction paths in oxidation of benzyl alcohol (BzOH) (see [7])



reaction, the formed aldehyde, BzO may also react with oxygen and with the original BzOH to form BzOOBz (reaction D) [7, 9, 11–13]. Further on, disproportionation reactions may also take place. Namely, from two BzOH molecules BzO and toluene (BzH) may be formed [11], or, in other way, BzOH and benzoate anion may be formed from two aldehydes in presence of strong base (Cannizzaro reaction).

The catalytic cycle of oxidation of BzOH in the process A is completed in three stages. First, the deprotonation of BzOH takes place by promotion of the basic -OH groups of the support or with OH^- in the solution. The second step, the β -hydrogen elimination from the formed alkoxy intermediate proceeds on the metallic gold surface, the BzO product is formed in this stage. The cycle is closed in the third step by removing the bonded hydrogen from the gold surface in the reaction with oxygen or with OH^- [10] by forming water. Kinetic models were also constructed and verified for the description of the mentioned complete cycles of BzOH oxidation in A–D reactions [3, 7, 12, 13].

The strong dependence of the turnover frequency related to surface Au atoms (TOF) on the size and shape of nanoparticles in BzOH oxidation is reported in [14]. A steep increase of TOF is reported on the decrease of particle size in [9, 15]. The usage of the term TOF needs precaution, since TOF values strongly depend on the experimental conditions, and on the method by which they are deduced. In addition, they may change depending on the type of catalytic sites to which they are related [15–18]. For oxidation with gold nanoparticles, 6–9 nm optimal size is found in [19]. The simultaneous adsorption of oxygen strongly influences the performance: in the absence of oxygen, small particles are more active, whereas in the presence of O_2 , the larger ones exhibit better performance of ethanol oxidation [20]. CO probe molecule with Fourier transformed infrared spectroscopy (FTIR) detection is used preferably for the characterization of active sites on gold particles. The presence of apparent extra charges on metallic particles can also be identified from shifts of bands by in situ measurements [21]. The amount of the chemisorbed CO is also an important parameter, it can be determined quantitatively in equilibrium with gas phase by pulse and frontal chromatography methods [22, 23]. It is also worth mentioning that the modification of gold with a second alloying element may significantly increase the activity in oxidation processes (e.g., with Pd [12] or with Ag [24] and Cu [25]). An important factor in the reaction is the coverage of atomic oxygen on the metallic particles as well [26]. Adsorption of oxygen on gold particles can dominantly be observed in the $\sim 50\text{--}400$ °C region [27].

The role of support is also crucial. It may participate in the sorption and H^+ extraction processes [28, 29]. The size and morphology of metallic particles also depend on the choice of support [1, 30]. Furthermore, certain oxides may also directly supply oxygen for the oxidation (e.g., CeO_2) [31, 32]. The basicity of the support is an advantageous feature, thus MgO is used in several cases [6, 28]. The binary, basic and acid features are even more favourable, as demonstrated with magnesium–aluminium hydrotalcite supports [9, 12, 29]. Other, less conventional oxide supports were also successfully applied in BzOH oxidation, e.g., zeolites [33], mixed $\text{SiO}_2\text{--Al}_2\text{O}_3$ oxides (halloysite, [34]) or various MgAl_2O_4 spinels in oxidation of glycerol [35].

The catalytic cycles during the oxidation of BzOH in reactions A–D are described in detail and are experimentally confirmed on Au/ Al_2O_3 in [7]. In the present study further

conventional supports (SiO_2 , MgO and MgAl_2O_4) beside Al_2O_3 are also compared in the oxidation of BzOH . Hydroxyapatite (HAP) is also included since it exhibits reverse SMSI, namely, different extent of encapsulation of gold particles occurs by HAP upon oxidation [36]. The main emphasis is laid on studying the acid–base properties, thus redox supports (CeO_2 , TiO_2 , V_2O_5 , etc.) are not involved. Two distant experimental conditions were selected. First, aerobic oxidation was carried out under mild conditions in xylene solvent at low-temperature ($60\text{ }^\circ\text{C}$) both in the presence and absence of K_2CO_3 additive. In the second series, solvent-free oxidation was accomplished under more severe conditions, in a closed autoclave by loading oxygen of 5 bar pressure at $150\text{ }^\circ\text{C}$. Gold nanoparticles with uniform distribution ($\sim 1.9\text{ nm}$) were prepared with aqueous phase reduction and stabilization by polyvinyl alcohol, PVA [37, 38] then adsorbed on the mentioned supports, and activated by calcination in air. The distribution and mean sizes of gold particles were determined with TEM measurements. The surface properties of gold nanoparticles were probed by diffuse reflectance FTIR spectroscopy (DRIFTS) measurements in CO and in $\text{CO} + \text{O}_2$ mixtures. The accessibility and fractions of active surface sites are experimentally determined by a novel method, by binary concentration pulse chromatography of CO with Kr adsorption with fast quadrupole mass spectrometry (QMS) detection. Acid–base properties are evaluated with CO_2 and NH_3 adsorptions followed by temperature programmed desorption. The initial stages of BzOH oxidation processes were determined from the $60\text{ }^\circ\text{C}$ measurements in xylene solvent and the activities are compared with the initial reaction rate method. The extents of conversions of BzOH and selectivities for BzO formation in solvent-free experiments performed at $150\text{ }^\circ\text{C}$ for 5 h in a closed autoclave were also determined. The results are interpreted in comparison with those of the former ($60\text{ }^\circ\text{C}$) series of measurements.

Emphasis is laid on the characterization and comparison of activity of gold on the different supports. Since the Au particle sizes vary in the samples compared, gold surface normalized activities are used (instead of the debated term of TOF [15–18]). Thus, conversion rates of BzOH are related to two types of accessible gold atoms. First, the activity is normalized to the total number of gold atoms present on the geometric surface of Au particles, geometric surface normalized activity, GSNA, is used. In the second variant, only the number of active sites enable to adsorb CO is considered, active site-normalized activity, ASNA, is applied. Initial conversion rates can reliably be derived from the initial period of reaction, when the extent of conversion is proportional to the time elapsed, these corresponding ASNA and GSNA values will be marked with “ini” subscript. Less exact activities which are deduced from a single conversion–time pair of values will be specified with “ave” (average) subscript.

Experimental

Preparation of catalysts

Samples were prepared by the adsorption of Au nanoparticles from Au sols on the different supports. Alumina, Al_2O_3 (Degussa Aluminium oxid C), silica, SiO_2 (Aerosil A200), magnesia, MgO (Aldrich), magnesium aluminate, MgAl_2O_4 (Aldrich)

non-porous nanopowders and hydroxyapatite ($\text{Ca}_{10}(\text{PO}_4)_6(\text{OH})_2$, HAP) were used for supporting Au nanoparticles. Specific surface area values were obtained from the suppliers (except HAP) and are shown in Table 1.

The preparation of HAP is described in [36], its specific surface area was determined with nitrogen physisorption measurements carried out at 77 K using a Thermo Scientific Surfer automatic, volumetric adsorption analyzer. Before adsorption analysis, the HAP sample was outgassed under vacuum for 2 h at 473 K.

Au sols containing nanoparticles of c.a. 1.9 nm mean diameter were produced from the mixture of 37.5 ml 6.0 mM HAuCl_4 , 45.0 ml 0.2 wt% PVA solution and 600 ml water by addition of 75 ml 25 mM NaBH_4 at about 0 °C [37].

Au sols in corresponding amounts were mixed with the supports to achieve the aimed Au loading. Appropriate amount of 0.08 wt% poly-diallyldimethylammonium chloride (PDDA) solution was also added to help the adsorption of metal particles (except in the case of alumina). The suspensions were stirred at room temperature for c.a. 2 h. The colorless supernatant was removed by filtration, the solid was washed by water thoroughly, then dried overnight at 80 °C. Catalysts were activated by calcination in air at 400 °C for 1 h removing the organic residues (PVA and PDDA) from the Au particles [39]. The gold loading of the catalysts was 3.0 wt% except Au/ SiO_2 which contained 1.8 wt% Au.

Sorption properties of supports: acid–base characteristics, density of surface OH groups

The basic and acid properties were characterized by CO_2 and NH_3 TPD measurements, respectively, using an Autochem 2920 (Micromeritics) apparatus equipped with a QMS analyser (Thermostar, Pfeiffer Vacuum). For CO_2 TPD measurements, 75 mg of supports were conditioned at 150 °C in Ar for 30 min, then the temperature was raised in 10 °C/min ramp to 400 °C and kept for 10 min. CO_2 was adsorbed from 2% CO_2/Ar mixture at 40 °C for 30 min, then the loosely adsorbed CO_2 was removed in Ar flow at 40 °C for 60 min. Temperature programmed desorption was performed by raising the temperature to 600 °C, with 10 °C/min ramp in Ar stream (30 ml/min). Desorptions of CO_2 ($m/z=44$), and water ($m/z=18$) were followed by QMS detection. The density of surface OH groups may also play role in the studied benzyl alcohol oxidation, thus the amount of the evolved water due to dehydroxylation was also monitored during the pretreatment of the supports.

For NH_3 TPD measurements, 75 mg of supports were conditioned at 150 °C in He for 30 min, then the temperature was raised with 10 °C/min ramp to 400 °C and kept for 10 min. NH_3 was adsorbed from 10% NH_3/He mixture at 40 °C for 30 min followed by removal of loosely adsorbed NH_3 in He for 30 min. The temperature programmed desorption of NH_3 was performed with the raise of temperature of 10 °C/min rate in He stream (40 ml/min). The amount of desorbed NH_3 was determined with QMS as NH_3 fragment ($m/z=16$).

Table 1 Specific surface area, acid–base properties derived from TPD measurements of CO₂ and NH₃ and extent of desorbed water on different supports

Support	Specific surface area (m ² g ⁻¹)	Basic and acidic properties			Water desorption	
		Desorbed CO ₂ ^a (μmol g ⁻¹)	Basic sites (μmol m ⁻²)	Desorbed NH ₃ ^b (μmol g ⁻¹)	Acidic sites (μmol m ⁻²)	150–400 °C (10 ⁻⁹ A s m ⁻²) ^c
MgO	~80	29	0.37	10	0.15	4.3
MgAl ₂ O ₄	53	28	0.53	230	4.4	4.4
HAP	73	71	0.97	200	2.7	0.95
Al ₂ O ₃	~100	15	0.15	200	2.0	1.6
SiO ₂	~200	2	0.01	10	0.05	0.34

^aUp to 600 °C^bUp to 550 °C^cIntegral of m/e = 18 ion current (A) versus time (s) related to surface area (m²)

Characterization of supported gold nanoparticles

Determination of particle size

Gold particle size distributions in the calcined catalysts were determined by measuring diameters of c.a. 300 particles on each catalyst from images obtained with a JEOL 3010 electron microscope operating at 300 kV.

CO adsorption followed by DRIFTS

A Nicolet iS50 FTIR spectrometer equipped with a Specac diffuse reflection accessory and an in situ chamber was used for the measurements. Spectra of adsorbed CO were collected at 35 °C in three versions: (i) on the catalysts calcined ex situ at 400 °C and after two further consecutive in situ pretreatments, (ii) oxidation, 400 °C/air/10 min and (iii) reduction, 400 °C 5% H₂ in Ar/30 min. Spectra were recorded after the oxidation pretreatment following 5 min exposure to 1% CO + 1% O₂/He gas flow, then also in 1% CO/Ar, and after reduction, first in 1% CO/Ar, then in 1% CO + 1% O₂/He. The pretreatments were carried out in the flow of the specified treating gas mixture, the heating rate was 10 °C/min. The cooling after treatment in air was carried out in the same synthetic air, whereas after treatment in 5% H₂-Ar samples were cooled in Ar. Spectra recorded at 35 °C after the pretreatment and prior the CO adsorption under Ar or air flow (in case of ex situ calcination or reduction pretreatments and oxidation, respectively) were used as reference for the log(1/R) representations. From the spectra recorded during adsorption, the CO gas spectrum was eliminated by subtraction. For comparison of the amounts of adsorbed CO the band intensities were considered, namely the integrals of log(1/R) bands were determined.

Determination of the amount of adsorbed CO with binary concentration pulse chromatography

Binary concentration pulse method was applied since the conventional pulse chemisorption technique cannot be used due to the weak adsorption of CO on Au. The amount of adsorbed CO from 1% CO + 1% Kr in Ar pulse was determined with fast QMS (Thermostar) detection in an Autochem 2920 apparatus. Subsequent to the in situ calcination treatment (400 °C/10% O₂ in He/1 h followed by cooling in air) 75 mg sample was exposed to 1% CO at 35 °C by a fast switch of the pure Ar flow to a 1% CO + 1% Kr/Ar stream (both 10 ml/min flow rate). After equilibrating CO between the surface and the gas phase for 10 min, the switch was reversed inducing the desorption of CO. The CO signal of the effluent gas mixture is delayed in comparison to that of the inert, non-adsorbing Kr at the front side of the binary pulse due to adsorption of CO. The area between the normalized Kr and CO signals is proportional to the amount of the adsorbed CO. In reverse, at the tail of the binary pulse the desorption of CO is delayed and the area between the normalized Kr and CO signals is proportional to the amount of the CO desorbed. Then, after 10 min on stream, the temperature was raised up to 400 °C by 10 °C/min rate (CO-TPD) to

complete the desorption. The amounts of adsorbed and desorbed CO were calculated by the difference between the integrals of the CO and Kr concentration versus time curves between the switch on and off time of CO + Kr/Ar, and between the CO + Kr/Ar switch off and the end of TPD, respectively. The CO and Kr concentrations were calculated from the intensities of $m/z = 28$ and 84 QMS signals.

The adsorption of CO on the bare supports is significantly smaller than on supported gold catalysts, but it is not negligible. Thus, amounts of adsorbed CO on pre-treated supports were also determined and are taken into consideration at the corresponding calculations.

Oxidation of BzOH

Experiments were carried out under two conditions:

- (i) The aerobic oxidation of BzOH was performed in xylene solvent (0.1 M BzOH) at 60 °C in a thermostated glass reactor with a magnetic stirrer and a reflux condenser. In a typical reaction 15 mg calcined catalyst and 400 mg K_2CO_3 was added to a mixture of 29.4 ml xylene and 0.3 ml dodecane as internal reference (in the case of Au/SiO₂, 25 mg catalyst was used to attain the same substrate/metal ratio). K_2CO_3 was used to prevent deactivation caused by benzoic acid poisoning (benzoic acid is possible trace contamination of benzyl alcohol and is the product of the reaction in further stages, too). The reaction was performed also without addition of base using the same reaction conditions in another series. The suspension was heated to 60 °C under stirring (1350 rpm), then O₂ was bubbled through the suspension with a flow rate of 150 ml/min (1 atm). After 20 min the reaction was started by adding 0.3 ml (2.9 mmol) benzyl alcohol (providing a substrate/metal molar ratio of ~1300). For analysing the reaction mixture ~0.2 ml samples were withdrawn with a syringe during the reaction in 10 min intervals. After the filtration of the catalyst and K_2CO_3 the liquid was analyzed by a CHROMPACK CP 9000 type gas chromatograph (GC) equipped with a FID detector using a CP-Sil-5-CB (50.0 m × 0.32 mm × 1.19 μm) capillary column. Beside benzaldehyde, only benzyl benzoate was detected as byproduct. The initial reaction rate was calculated from the first three points of the conversion curves (up to 30 min reaction time, linear region). $GSNA_{ini}$ and $ASNA_{ini}$ values were determined by dividing the initial reaction rate of BzOH conversion with molar amount of Au atoms located on the geometric surface of particles, and with molar amount of surface Au atoms able to adsorb CO molecules, respectively.
- (ii) Solvent-free oxidations were carried out in an autoclave equipped with a magnetic stirrer. In a typical procedure, 50 mg catalyst and 2 ml BzOH (corresponding to substrate/metal ~2500 molar ratio) were placed to the autoclave which was then flushed with 5 bar O₂ for five times, and loaded finally with 5 bar O₂. The autoclave was closed, then it was heated to 150 °C and kept for 5 h afterwards. The reaction was stopped by cooling the autoclave, then 0.05 ml dodecane as inner standard was added to 0.1 ml of the filtered reaction liquid and the mixture was diluted with 1 ml ethyl acetate. The

products were analyzed by gas chromatography–mass spectrometry (GC–MS) tandem, an Agilent 7890B instrument equipped with an on-column injector (260 °C), a FID detector (325 °C) and an HP-5 capillary column (30 m × 0.32 mm × 0.25 mm). Conversions and selectivities were calculated from these data. The average reaction rates during 5 h reaction were determined from conversions, from that average $GSNA_{ave}$ values were calculated.

Results and discussion

Acid–base properties of the supports

The acid–base properties of the supports were evaluated with CO_2 and NH_3 adsorption followed by TPD measurements (Fig. 1). Total amounts of CO_2 and NH_3 desorbed up to 600 °C and 550 °C, respectively, are shown in Table 1.

The characteristics of the various supports are rather different from the aspect of basicity. In the literature, the basicities of oxides are classified in three groups concerning the strength of base sites. The weak sites are related to surface hydroxyl groups, the medium ones to $M^{n+}-O^{2-}$ pairs, the strong ones to low coordination O^{2-} ions [40]. SiO_2 hardly exhibits any adsorption/desorption of CO_2 . The basicity of alumina is also weak, most of desorption has taken place below 150 °C, the amount of evolved CO_2 is small. The sorption of CO_2 and basic strength on MgO is more expressed. It is worth noticing that the evolution of CO_2 proceeds in three steps. The first two of them appear in two overlapping peaks with a maximum of desorption around 140 °C, and a shoulder around 100 °C. A smaller desorption peak appears around 450 °C as well. It can be supposed that CO_2 released around 100 °C originates from carbon dioxide attached to the –OH groups forming bicarbonate, whereas the CO_2 evolution between 140–400 °C and above 400 °C is related to decomposition of bidentate and the more stable unidentate carbonates, bonded to $Mg^{2+}-O^{2-}$ pair sites and isolated O^{2-} ions on surface edges or corners [41]. A similar amount

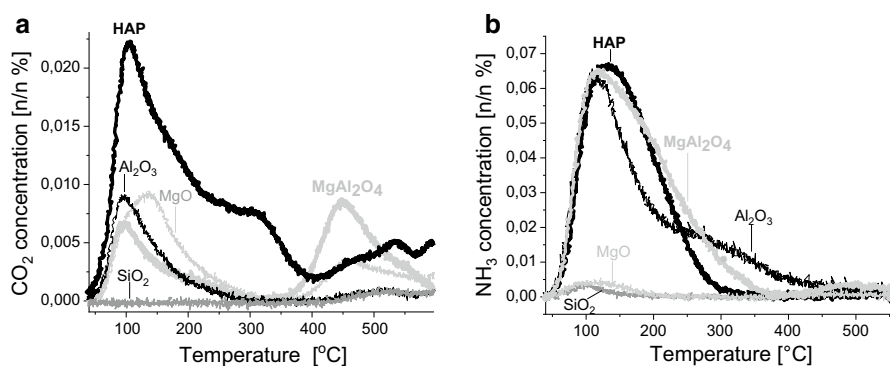


Fig. 1 Acid–base properties of the supports: CO_2 -TPD for basicity (a, left), NH_3 -TPD for acidity (b, right) characterization

of CO_2 is desorbed from MgAl_2O_4 , reflecting a higher surface density, and its larger part is related to stronger basic sites with desorption around 450°C . The basicity of HAP is the highest among the studied supports. The dominant part of CO_2 is evolved around 120°C and a significant part is still originated from stronger basic sites with release around 300°C and above 400°C . Without distinction of strengths, the overall specific basicities are in the order $\text{SiO}_2 < \text{Al}_2\text{O}_3 < \text{MgO} \approx \text{MgAl}_2\text{O}_4 < \text{HAP}$ (Table 1).

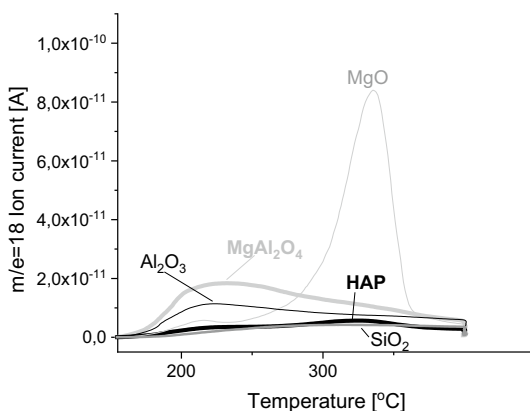
The acidities of various supports are also characteristically different (Fig. 1b). The adsorption of ammonia on magnesia and silica is negligible. Acidities of MgAl_2O_4 , HAP and Al_2O_3 are more expressed. The desorption of NH_3 results in broad peaks for MgAl_2O_4 and HAP, whereas the strengths of acidic sites were distinctly different on alumina, the presence of weaker sites is reflected in a low temperature peak centered around 120°C , stronger sites result in a broader $200\text{--}350^\circ\text{C}$ desorption. Similar NH_3 desorption patterns are reported for catalysts on these supports e.g., in [9]. Specific acidity data are shown in Table 1.

Sorption/desorption of water, density of surface hydroxyls

The desorption of water from the supports was also traced in our study, since presence of water and hydroxyl groups may significantly accelerate the processes of BzOH oxidation and water is formed itself in the reaction. The signal of desorbed water ($m/z=18$) was traced by QMS detection of the TPD in Ar between 150 and 400°C , subsequently to 30 min pretreatment in Ar at 150°C . The signal originates primarily from surface OH groups since the physisorbed water is removed with the applied pretreatment (Fig. 2). Integrated amounts of $m/e=18$ signal versus time in the $150\text{--}400^\circ\text{C}$ region of the curves in Fig. 2 are collected in Table 1 as well. Thus, an indication on the amounts of the surface density of hydroxyls on the various supports can be obtained and compared.

The largest evolved amount of water is obtained from MgO support. Only a small amount appears in the $200\text{--}250^\circ\text{C}$ range, characteristic otherwise for the dominant desorption on MgAl_2O_4 and Al_2O_3 . The overwhelming desorption takes

Fig. 2 Desorption of water from different supports ($m/z=18$ QMS signal), during pretreatment in Ar in the $150\text{--}400^\circ\text{C}$ range



place at 300–350 °C, in a typical temperature range observed for $\text{Mg}(\text{OH})_2 \rightarrow \text{MgO}$ conversion on small particles [42] (Fig. 2). Thus, OH groups on MgO are probably bonded more strongly. On HAP and SiO_2 the water evolution is negligible compared to the other supports. The amounts of the evolved water related to unit surface area can also be estimated on the different supports (Table 1). The density of surface OH groups decreased on the various supports in the following order: $\text{MgAl}_2\text{O}_4 \approx \text{MgO} > \text{Al}_2\text{O}_3 > \text{HAP} > \text{SiO}_2$. In a consecutive TPD from 400 to 800 °C, an additional, but significantly lower amount of water evolved (not shown) due to further dehydroxylation. However, considering the sum of hydroxyl eliminated between 150 and 800 °C, the order of supports does not change.

Particle size distributions, average particle sizes, dispersions

From TEM images (representative ones are shown in the Fig. 3) the gold particle size distributions (Fig. 3, insets) of the calcined (400 °C/air/1 h) catalysts were determined. The mean particle diameter (d_m) was calculated by using the $d_m = \sum d_i n_i / \sum n_i$ formula where n_i is the number of particles of diameter d_i (Table 2). Dispersions were also estimated with geometrical approximation (similarly to [3, 14, 19]). Spherical shape was assumed for the gold particles, and for the estimation of the number of surface gold atoms 11.5 gold atom per unit area (nm^{-2}) surface density value was applied [43]. In accordance, the dispersion (D) of gold was calculated by the $D = 1.17 (\sum d_i^2 n_i / \sum n_i) / (\sum d_i^3 n_i / \sum n_i)$ formula, where d is expressed in nm. It is worth noticing that the original small size of the gold nanoparticles is preserved only on the Al_2O_3 support. Certain agglomeration has taken place during the 400 °C calcination on all the other supports, particularly on MgO. It is worth noticing that the crystal shape of stable gold nanoparticles varies with the size [44]. However, the influence of this effect is neglected in our evaluation.

CO adsorption (DRIFTS)

Concentration and properties of the low coordinated Au sites, generally the most reactive ones can be characterized by comparing the adsorption of CO on various catalysts as reflected in DRIFT spectra. As for the effect of particle size in the oxidation of alcohols, the reports are controversial. There are publications suggesting the steep increase of TOF with decreasing gold particle size [9, 14, 15], in contrast, a volcano shape size dependence is also reported with TOF maximum at around 6–9 nm particle size in [19].

The redox steps of β -hydride elimination and the removal of the separated hydrogen with oxygen in a subsequent stage on the surface of gold nanoparticles is crucial in the catalytic cycle of BzOH oxidation. Thus, the effects of redox pretreatments on the supported gold nanoparticles were monitored by measuring the CO sorption under two conditions at room temperature. First, the co-adsorption of CO and oxygen was performed from 1% CO + 1% O_2 /He mixture on the ex situ calcined sample and on samples exposed to in situ oxidizing pretreatments. Second, CO sorption from 1% CO/Ar mixture was measured. After the in situ reducing pretreatment, the

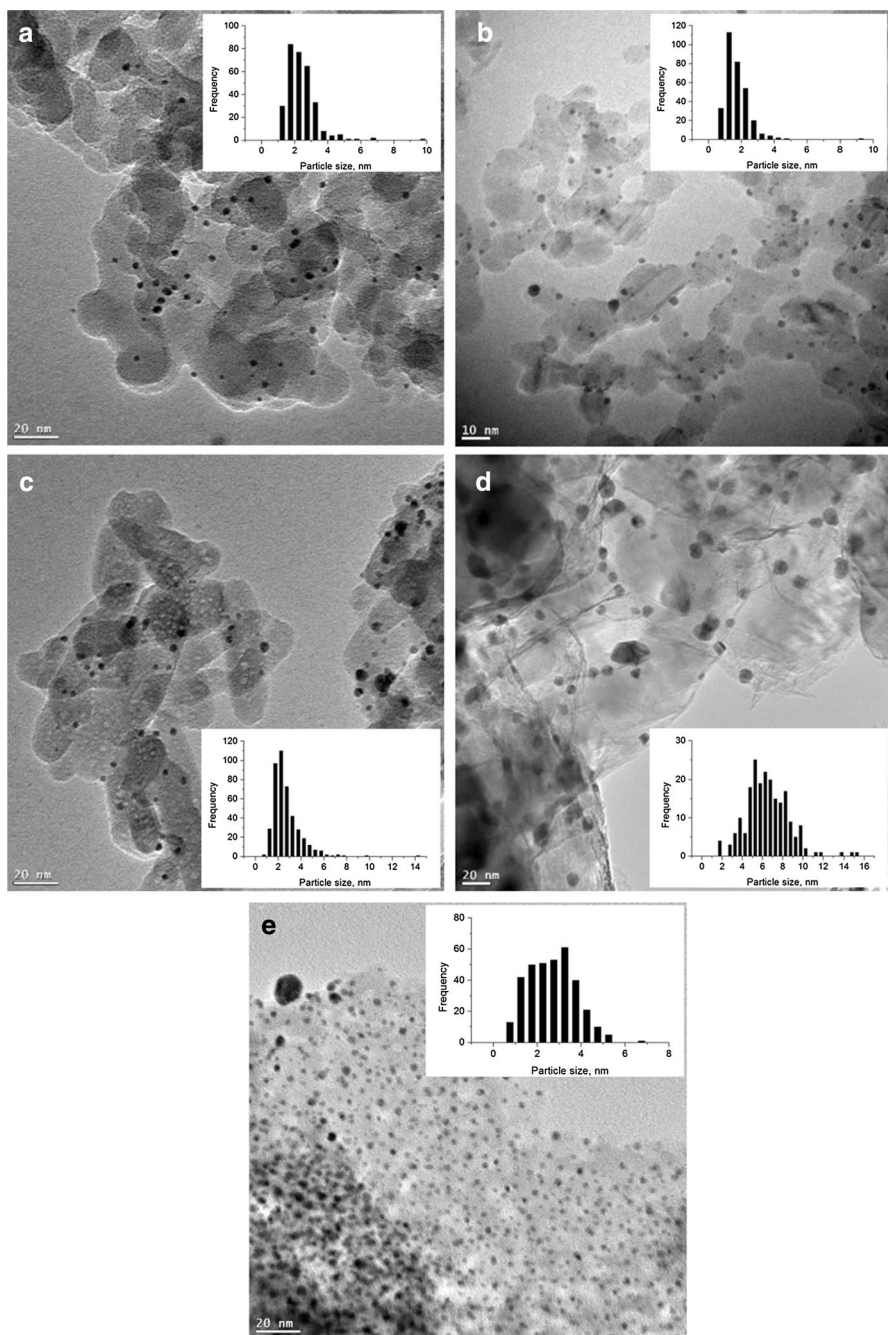


Fig. 3 Representative TEM images of the various calcined catalysts. **a** Au/SiO₂, **b** Au/Al₂O₃, **c** Au/HAP, **d** Au/MgO, **e** Au/MgAl₂O₄. The corresponding particle size distributions are shown in the insets

Table 2 Mean diameter and dispersion values of Au particles on various supports

	Au/SiO ₂	Au/Al ₂ O ₃	Au/HAP	Au/MgAl ₂ O ₄	Au/MgO
Au loading (wt%)	1.8	3.0	3.0	3.0	3.0
Mean diameter (nm)	2.4	1.7	2.7	2.7	6.5
Dispersion (%)	35	43	27	34	15

sorption of CO alone preceded the co-adsorption of CO + O₂. Special attention was devoted to monitoring the blue shift occurring in the band of carbon monoxide co-adsorbed with O₂. The results are summarized in Table 3, corresponding spectra are shown in Fig. S1 (Supplementary Material).

In general, blue shift (increase of wave number) appears when oxidized samples are compared to reduced metallic ones [21, 45, 46]. Another similar process, the co-adsorption of CO and O₂ on metallic gold may also result in certain blue shift. The blue shift is an indication of the appearance of a certain electron deficiency (partial positive charge) on the particles. This positive charge may influence the reactivity of particles [47]. In the evaluation of the observed band shifts, the red shift induced by the increase of CO surface coverage typical on gold also must be taken into consideration. The effect of the co-adsorption of O₂ with CO on the CO band position can be observed reliably on the reduced samples. The increase of the extent of this phenomenon is in the Au/SiO₂ < Au/MgAl₂O₄ < Au/Al₂O₃ < Au/MgO < Au/HAP order. The differences in the sizes of gold nanoparticles on the various supports (Table 2) may influence the density of the coordinatively unsaturated gold sites on which co-adsorption of CO and O₂ is taking place. Furthermore, it is also worth considering that the size of Au particles on MgO is the largest however, a significant blue shift is still observed.

It is worth emphasizing that the BzOH oxidation reaction was performed with catalysts activated by calcination previously, i.e., on gold particles with partly oxidized surfaces. This is shown by the appearance of a larger frequency band (2123–2126 cm⁻¹) with decreasing intensity ratio on Au supported on SiO₂,

Table 3 Wavenumbers of CO band maxima in DRIFT spectra of adsorbed CO at room temperature after various pretreatments of supported gold catalysts

Treatment (400 °C)	Probe gas	Wavenumbers of CO band maxima (cm ⁻¹)				
		Au/SiO ₂	Au/Al ₂ O ₃	Au/HAP	Au/MgAl ₂ O ₄	Au/MgO
Air/ex situ	1% CO in Ar	2110, 2126 sh	2102, 2123 vw sh	2108	2106	2102
Air/in situ		2115, 2126 sh	2107, 2123 vw sh	2111	2110, 2123 sh	2105
5% H ₂ /Ar		2109	2105	2108	2107	2104
Air/ex situ	1% CO + 1% O ₂	2126, 2112	2106, 2123 w sh	2120	2110, 2123 sh	2105
Air/in situ	in He	2126, 2113 sh	2112, 2123 w sh	2120	2123, 2111 w sh	2110
5% H ₂ /Ar		2112	2110	2116	2110	2110

sh shoulder, *w sh* weak shoulder, *vw sh* very weak shoulder

MgAl₂O₄ and Al₂O₃ overlapping with the band assigned to the CO co-adsorbed with O₂ on metallic Au sites (2110–2113 cm⁻¹). On Au/HAP, the simultaneous presence of this two CO bands cannot be recognized, but a small blue shift (4 cm⁻¹) compared to the band of the co-adsorbed CO + O₂ on the reduced sample can be observed. In the case of Au/MgO, no significant difference can be observed between the CO-band positions recorded on the in situ calcined and reduced state.

On another aspect, the intensities of CO_{ads} bands are distinctly different on the various catalysts (Fig. S1). These intensities can be correlated to the amounts of adsorbed CO, a comparison of them is presented in Table 4. The order of them on catalysts with the corresponding supports is Al₂O₃ > SiO₂ ≈ MgAl₂O₄ > HAP > MgO. That is in good correlation with the particle sizes, except Au/HAP on that the CO band intensities are smaller than expected. There is one order of magnitude difference between the highest and smallest peak areas (Al₂O₃ and MgO, respectively—Table 4). The reduction/oxidation pretreatment has only a minor influence on the CO band intensities, in particular, the reductive pretreatment results in some decrease of the CO bands on Au/HAP, and larger on Au/MgO that might be due to some further sintering. Au/Al₂O₃ is the outermost as for the amount of adsorbed CO. The blue shift is the smallest on Au/MgO after oxidation, while on Au/HAP is the largest on the O₂ co-adsorption with CO (Table 3).

Determination of the amount of adsorbed CO from binary concentration pulse chromatography

DRIFTS CO measurements do not provide exact information on the amounts of the adsorbed CO. A more accurate technique, the binary concentration pulse chromatography with fast mass spectrometric detection can be applied for quantitative measurements. The method is demonstrated in Fig. 4a in the case of Au/Al₂O₃ catalyst. The Ar flow through the catalyst was changed instantly to 1% CO + 1%

Table 4 Amounts of CO adsorbed on gold calculated from intensities of DRIFTS bands (2150–2050 cm⁻¹) and amounts of adsorbed and desorbed CO from gold determined by binary concentration pulse chromatography and the derived partial coverage of the surfaces of gold nanoparticles in the various calcined samples

	DRIFTS CO _{ads} band intensity	CO _{ads} mol CO/mol Au	CO _{des} mol CO/mol Au	CO _{des} mol CO/mol Au ^a _{surf}
Au/SiO ₂	6.5 ^b	0.020	0.026	0.07
Au/Al ₂ O ₃	12.2	0.153	0.066	0.15
Au/HAP	2.0	0.018	0.009	0.03
Au/MgAl ₂ O ₄	5.0	0.052	0.027	0.08
Au/MgO	1.3	0.006	0.004	0.03

^aAu_{surf} is calculated by the multiplication of gold concentration of the samples (mol/g_{cat}) by the dispersion data calculated from the particle diameters (Table 2)

^bThe band intensities measured on the 1.8 wt% Au/SiO₂ were normalized to 3 wt% Au content for better comparisons with the other catalysts

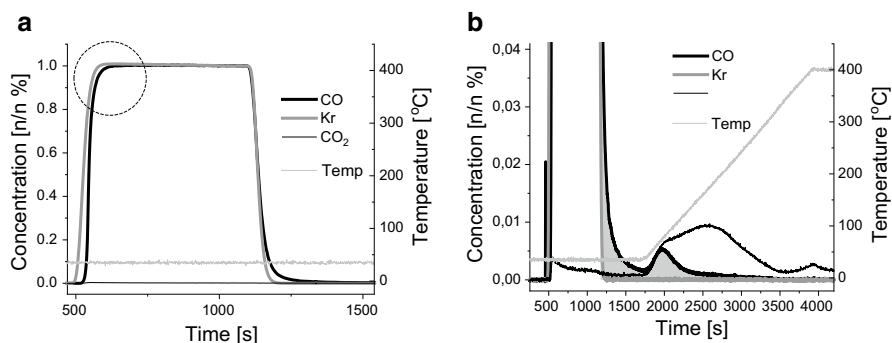


Fig. 4 Binary concentration pulse chromatography with mixed 1% CO+1% Kr pulses in Ar stream for determination of the amount of adsorbed CO on Au/Al₂O₃ sample, with a possible CO+Au_nO→CO₂+Au_n process (encircled, left, **a**), and the enlarged (ca. 25 times) bottom portion of the concentration jump on the left supplemented with the desorption in the subsequent TPD (right, **b**)

Kr in the Ar mixture at 35 °C. The signal of CO is delayed in a certain extent as compared to the non-adsorbing Kr. After 10 min, having the sorption processes equilibrated the flow of 1 + 1% CO + Kr mixture is abruptly stopped, then the signal of CO related to that of Kr is delayed again. The delay in the ascending side is proportional to the amount of adsorbed CO. There is a further lag in the CO signal at the beginning of top of the Kr + CO pulse (encircled in the Fig. 4a), it may be partly related to a certain reduction of the Au_nO species formed in the in situ calcination prior to the exposure to the CO + Kr pulse. Thus, the total amount of spent CO is added from contributions of CO_{ads} and CO + Au_{n,surf}O → CO₂ + Au_{n,surf}. The carbon dioxide formed can be fixed on the support depending on its basicity (see also in Fig. 1a). On the descending side, the delay of the CO signal appears only on the bottom part of the pulse, however it is tailing due to the slow desorption from gold. The desorption process can be facilitated with a TPD of CO as shown in Fig. 4b. Since the amount of the desorbed carbon monoxide in the descending step, CO_{des}, is exempt from other processes, it can be considered for the estimation of the amount of chemisorbed carbon monoxide. In correspondence with the mentioned CO₂ formation, the MS signal of CO₂ desorbing from the support could also be detected during the TPD, as shown in Fig. 4b. The adsorption of CO on pretreated bare supports was also determined. Its extent is much smaller than on supported gold catalysts, but it is not negligible. Thus, it was subtracted from that measured for the corresponding supported gold catalysts providing the CO amount adsorbed on Au sites. The amount of CO adsorption and desorption on gold related to 1 mol Au content in the different samples are summarized in Table 4 and compared with the IR band intensities of CO adsorbed on the in situ calcined samples.

It is worth to notice that the correspondence between the data for the log(1/R) band intensities of adsorbed CO obtained from the DRIFTS and binary concentration pulse chromatography methods is fairly good. Namely, the order of the catalysts from the point

of view of the adsorbed CO is $\text{Au}/\text{Al}_2\text{O}_3 > \text{Au}/\text{MgAl}_2\text{O}_4 > \text{Au}/\text{SiO}_2 > \text{Au}/\text{HAP} > \text{Au}/\text{MgO}$ by both of the methods.

A simple geometric approximation was used to estimate the number of surface gold atoms as mentioned in the beginning of the Results and Discussion chapter in connection with dispersion data presented in Table 2. In the knowledge of the quantitative amounts of adsorbed CO on gold the fractional coverage of gold nanoparticles can also be estimated by dividing the recent desorption data with the amount of surface Au atoms. The resulting data are shown in the last column of Table 4. In agreement with the expectations, the fractional coverages are in correlation with the mean particle sizes. Only the coordinatively unsaturated gold atoms on the surface of nanoparticles are able to adsorb CO, their proportion is increasing with the decrease of the particle size. The largest fractional coverage is found for $\text{Au}/\text{Al}_2\text{O}_3$ (15%) in agreement with the smallest average particle size found for this catalyst (~1.7 nm, Table 2). The medium sizes on SiO_2 , MgAl_2O_4 and HAP (2.4, 2.7 and 2.7 nm,) are reflected in medium fractional coverages in case of the two former support (7 and 8%). Surprisingly, it is much lower on HAP (3%). This latter value may be explained by the reverse SMSI effect on Au/HAP on calcination reported in [36]. Further on, particles with the largest Au size on MgO (~6.5 nm mean diameter) exhibit similarly low fractional surface coverage (3%) as found on HAP.

Aerobic oxidation of benzyl alcohol in xylene solvent at 60 °C in absence of K_2CO_3

The initial reaction rates of BzOH conversions were determined from the slopes in the linear sections of the conversion–time diagrams (the first 3 points in Fig. 5a and c), similarly as for example in [14]. The order of the activity of gold catalysts on various supports in absence of K_2CO_3 is: SiO_2 (~0) < HAP < MgO < $\text{Al}_2\text{O}_3 \approx \text{MgAl}_2\text{O}_4$. In the initial stage of the reaction the spread of activities on the different catalysts is rather broad, the conversion is modest (uppermost 7%) and in correspondence, the selectivity for BzO exceeds 95%. The sole detectable side product is the ester, BzO-OBz. Thus, dominantly only reaction A has taken place (Scheme 1). The two important stages in this oxidation cycle are the deprotonation promoted by the support, and the β -hydride elimination taking place on the gold nanoparticles [7].

GSNA_{ini} and ASNA_{ini} values are calculated in Table 5 from initial reaction rates by considering the concentration of either surface Au atoms (Au concentration, mol/g_{cat} multiplied by dispersion) or active, CO adsorbing surface gold atoms (obtained from the last column of Table 4), respectively. As mentioned earlier, from the aspect of size dependence of benzyl-alcohol oxidation controversial reports can be found, namely either monotonous increase of TOF with the size reduction of gold [9, 14, 15, 29] or volcano type dependence with activity maximum at 6–9 nm Au sizes [19]. In the former case the comparison of ASNA_{ini} is the more reliable to compare the influence of different support. If the latter case is valid GSNA_{ini} values are in better contrast taking into account all the surface Au atoms. However, the joint effect of particle size and type of support cannot be separated, rather the comparison of the catalysts of the similar size Au particles gives reliable information on the support effect. From the aspect of further comparisons it is worth noticing that in most publications the reported TOF

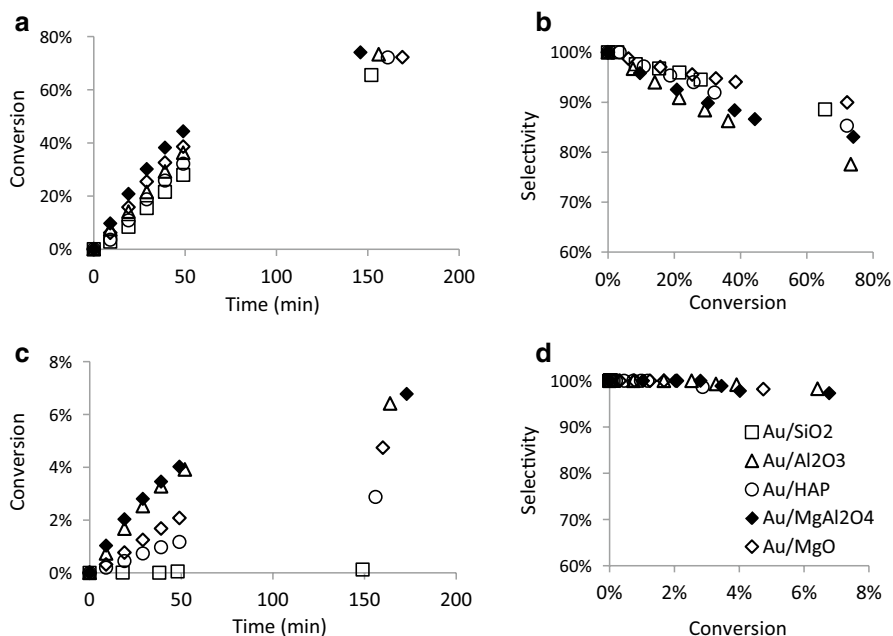


Fig. 5 Conversion versus reaction time (**a**, **c**, left) and selectivity versus conversion (**b**, **d**, right) curves of benzyl alcohol oxidation on supported Au catalysts, in presence (**a**, **b**, top) and in absence (**c**, **d**, bottom) of K_2CO_3 . (Note the different scales on the conversion axes.)

Table 5 Comparison of normalized conversion rates from measurements performed (i) at 60 °C in xylene solvent and (ii) 150 °C, 5 bar O_2 , 5 h

Conditions	(i) In xylene solvent, 60 °C, 1 bar O_2				(ii) Solvent-free, 150 °C, 5 bar O_2
	In absence of K_2CO_3		In presence of K_2CO_3		In absence of K_2CO_3
	GSNA _{ini} s ⁻¹	ASNA _{ini} s ⁻¹	GSNA _{ini} s ⁻¹	ASNA _{ini} s ⁻¹	GSNA _{ave} ^a s ⁻¹
Au/SiO ₂	0	0	0.28	3.97	0.63
Au/Al ₂ O ₃	0.04	0.28	0.36	2.41	0.16
Au/HAP	0.02	0.65	0.44	14.81	0.47
Au/MgAl ₂ O ₄	0.06	0.69	0.64	8.00	0.40
Au/MgO	0.05	1.56	1.22	40.8	0.83

^aThese data are obtained from measurements with high conversions (see Table 6)

values are related either to all metal atoms or to all surface atoms, respectively, which may result in a certain ambiguity [16, 17].

The interpretation of catalytic processes taking place in absence of K_2CO_3 may primarily be related to the basicity and to the density of active sites on gold particles. In particular, silica is neutral, the starting activation of BzOH for the catalytic cycle probably does not take place, GSNA (and ASNA) are practically zero. HAP,

the support of the next catalyst in the increasing order of activities, possesses the highest specific basicity (Table 1). However, from the aspect of the number of Au sites adsorbing CO, as well as the accessible Au surface are surprisingly low, likely because of the supposed partial encapsulation of Au particles by HAP [36]. The balance of basicity and accessibility results probably in the modest $GSNA_{ini}$, but similar $ASNA_{ini}$ as the most active Au/MgAl₂O₄ of similar gold size. Alumina, the next support in the order of activities of catalysts, exhibits only small overall basicity. In the relatively good performance probably the smallest particle size with highest concentration of low coordinated sites plays important role (1.7 nm, Table 2). The better performance of the Au/MgO catalyst can probably be related to the better specific basicity of the support (Table 1). The best $GSNA_{ini}$ is found on MgAl₂O₄, its specific basicity is similar to that of MgO, connected to higher surface density. From the point of view of $ASNA_{ini}$ Au/MgO is the most active by far (due to the large particle size with less low coordinated sites).

Aerobic oxidation of benzyl alcohol in xylene solvent at 60 °C in presence of K₂CO₃

As expected, addition of K₂CO₃ to the reaction mixture in stoichiometric amount results in a 10–20 fold increase in the conversion rates compared to those found in absence of K₂CO₃ since the added base increases the deprotonation of BzOH [8] and eliminates the poisoning effect of the BzOOH [7]. The apparent conversion rates are rather similar to each other in the SiO₂ < HAP < Al₂O₃ < MgO < MgAl₂O₄ increasing order (Fig. 5a). The extents of conversions during 3 h exceed 60% in all cases, the corresponding BzO selectivities fall into the 77–90% range, thus formation of BzOOBz has also taken place in modest extent rather via reaction D (due to base addition B + C route is less probable in Scheme 1 [7]). The BzOOBz selectivity increases with increasing acidity of the supports.

After having the Au dispersions taken into account the differences between the $GSNA_{ini}$ values are maximum ca. 4.5 fold, their order is SiO₂ < Al₂O₃ < HAP < MgAl₂O₄ < MgO (Table 5). In the later stage, considering only the extent of the reactive surface gold atoms, the previous order of activities changes, the difference between the smallest and largest activities ($ASNA_{ini}$) exceeds even an order of magnitude. In the case of reactions performed with K₂CO₃ addition, the role of basicity of supports is less expressed, the acidity of supports should also be considered and probably the balance of the acidic versus basic strengths is also an important parameter. In agreement, Au/SiO₂ and Au/Al₂O₃ are the least active with respect to both $GSNA_{ini}$ and $ASNA_{ini}$. Alumina support exhibits strong acidic sites (Fig. 1b). Furthermore, it should be added that the average gold particle size on this catalyst is the smallest (1.7 nm), maybe the number of neighboring Au sites is already insufficient for the appropriate BzOH adsorption resulting in a drop of activity as observed in [14]. SiO₂ is neutral, being neither acidic nor basic (Fig. 1), thus the activity of Au/SiO₂ catalyst can be considered as the one originated primarily from the gold nanoparticles with only minor influence of the support. The next more active catalyst is Au/MgAl₂O₄ or Au/HAP according to $GSNA_{ini}$ and $ASNA_{ini}$, respectively. However, Au/HAP can be regarded to be better since its $GSNA_{ini}$ is

underestimated as not all surface Au is accessible. MgAl_2O_4 has the largest acidity and the second largest basicity, for HAP the opposite is observed. Thus, the activity of gold might be better on these supports than on alumina and silica. The activity of Au/MgO is the best, its GSNA_{ini} and ASNA_{ini} values outperform those of all the other catalysts by ca. 2–4 and 5–10 times, respectively. MgO principally a basic support, the size range of gold particles on it is the same as was found to be the most active in Haider et al.'s [19, 48] reports, too.

Additionally, it should be emphasized that water as by product is formed in significant amount in the reaction at large conversions (e.g. 60% conversion may result in formation of 20–25 mg water which strongly exceeds the mass of 15 mg catalyst present in the reaction mixture). Thus, for the deeper interpretation of the promoting effect of K_2CO_3 , the promoting effect of the water should also be considered (discussed in more detail later).

Solvent-free oxidation of benzyl alcohol in autoclave under 5 bar O_2 at 150 °C

The oxidation of the BzOH substrate under these conditions was carried on for 5 h. The extents of conversions of BzOH and the selectivities of products are collected in Table 6, the corresponding acid–base properties, conversions and yields of various products are illustrated in Fig. 6.

The reaction conditions applied in solvent-free media with 5 bar starting load of oxygen at 150 °C were distinctly different from those of the atmospheric experiments carried out in xylene solvent without K_2CO_3 additive. Almost complete (> 85%) conversions were observed (except Au/ Al_2O_3 with only 47%). The starting amount of oxygen provided by the 5 bar load had been depleted almost completely in the reaction with the 2 ml BzOH substrate at these high conversions. Thus, the yields shown in Fig. 6 can be considered as corresponding to occasional equilibria established in the available pool of components.

Further on, it should be noticed that presence of the other reaction product, water, may also play a significant role. Namely, it promotes selectively the formation of BzOOH from BzO [5]. Considering ca. 80% conversion in average, presence of ca. 20 mmol (360 mg) water can be expected at the final stage, which is a large excess compared to the used 50 mg supported catalyst. The differences in the observed yields of products can probably be attributed to the different extents of completion

Table 6 Conversions and selectivities of BzOH oxidation (solvent-free, 5 bar O_2 , 150 °C, 5 h)

Catalyst	Conversion of BzOH (%)	Selectivity (%)		
		BzO	BzOOH	BzOOBz
Au/MgO	85	47	29	24
Au/MgAl ₂ O ₄	94	31	21	48
Au/HAP	87	66	14	20
Au/Al ₂ O ₃	47	93	6	1
Au/SiO ₂ ^{a)}	91	29	56	15

^{a)}1.8 wt% Au

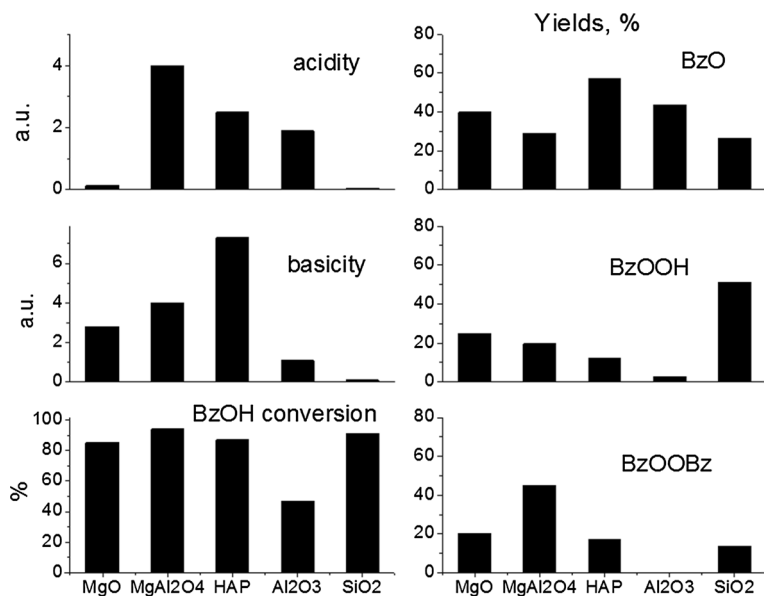


Fig. 6 Overall acidity and basicity (a.u.) of supports and detected conversions of BzOH (left) and yields of formation of BzO, BzOOH and BzOOBz (right) on various samples in solvent-free conditions after 5 h reaction at 150 °C with 5 bar O₂ load

of processes shown in Scheme 1, due to the various acid–base properties and to the extents of water present on the support during reactions.

Comparison of the activities determined under different experimental conditions

The activities determined under the different experimental conditions can be compared in Table 5. However, a comparison of $GSNA_{ini}$ in the case of measurements in xylene, and $GSNA_{ave}$ values obtained in the solvent-free reaction at 150 °C for 5 h needs precaution since the conversions in these latter tests were high, the proportional conversion-reaction time range of reactions had already been passed over. Furthermore, deactivation might have been taken place [49], so these values are probably underestimated as compared to a corresponding $GSNA_{ini}$.

Recent results obtained under the solvent-free conditions are valuable from practical aspects, providing a guide for practical applications. Selectivities at close to total conversion are worth also to compare. However further detailed investigation of the kinetics and mechanism is needed for better understanding the markedly different performances.

A comparison of our catalysts with literature ones in solvent-free conditions is presented in Table 7. The activities are characterized by the average rate of BzOH conversion during reaction time given related to 1 mol Au atoms (both surface and bulk) as mostly used (as TOF) in the cited papers. It should be noted that greater number of supports are compared in the report of Choudhary et al. [50], the

Table 7 Comparison of performance of various catalysts in solvent-free oxidation of benzaldehyde

Catalyst	Au particle size (nm)	Temp (°C)	P(O ₂) (MPa)	Time (h)	Conversion (%)	Selectivity ^a (%)	Activity mol _{BzOH} /h/ mol _{Au} (h ⁻¹)	Ref.
Au/Al ₂ O ₃	1.7 ± 0.8	150	0.5	5	47	93	247	This work
Au/MgO	6.5 ± 2.1	150	0.5	5	85	47	446	This work
Au/HAP	2.7 ± 1.3	150	0.5	5	87	66	457	This work
Au/ MgAl ₂ O ₄	2.7 ± 1.1	150	0.5	5	94	31	494	This work
Au/SiO ₂	2.4 ± 0.9	150	0.5	5	91	29	797	This work
Au/CeO ₂ - RRCe	4.5	150	0.5	8	37	72	288	[31]
Au/CeO ₂	n.a.	100	0.2	3	3.4	100	215	[49]
Au/SiO ₂	n.a.	100	0.2	3	1.9	100	343	[49]
Au/SiO ₂	n.a.	100	0.6	3	4.7	92	848	[49]
Au/ZrO ₂	4.5 ± 1.2	130	0.15	5	51	87	192	[50]
Au/Al ₂ O ₃	3.6 ± 1.1	130	0.15	5	69	65	125	[50]
Au/MgO	8.9 ± 0.7	130	0.15	5	51	86	81	[50]
Au/MgO	9	120	0.1	5	56	95	88	[28]
Fe ₃ O ₄ /Au/ SiO ₂	11	140	0.1	4	49	97	71	[51]

^aSelectivity of benzaldehyde

activities scatter between 30 and 192 (mol BnOH/h/mol Au). Our catalysts exhibit rather good performance in oxidation of BzOH. The good activities are probably connected to the stabilization of gold particles in small size range. The selectivities to benzaldehyde on our samples at 85% or higher conversions are significantly smaller in comparison to other catalysts in Table 7, where the extents of BzOH conversions were much lower.

Summary

Monodisperse PVA stabilized gold particles of around 2 nm diameter were prepared and adsorbed on non-redox supports of various acid–base properties, namely on SiO₂, Al₂O₃, MgO, MgAl₂O₄ and HAP. The next activation with calcination at 400 °C results in sintering of gold in different extents. The samples were characterized by TEM, CO adsorption followed by DRIFTS and measured by binary concentration pulse chromatography. The basicity and acidity of the supports were probed by CO₂- and NH₃-TPD, respectively.

Catalytic benzyl alcohol oxidation tests were performed under three experimental conditions. In the first and second version the reaction was carried out in xylene solvent at atmospheric pressure of oxygen at 60 °C, either in presence or in absence of K₂CO₃ in stoichiometric amount. Conversion and selectivity were determined in

dependence of reaction time. In the third version the reaction was carried out in solvent-free condition, under 5 bar O_2 starting pressure at 150 °C, the conversion and selectivity were measured after 5 h reaction. In the first and second case the activities of catalysts were derived from initial conversion rates related either to the number of gold atoms located on the geometric surface of particles ($GSNA_{ini}$) or to the number of active surface sites ($ASNA_{ini}$). The latter number of the active sites on gold particles was determined from CO adsorption followed by binary concentration pulse chromatography. In the third version of experimental conditions, the average reaction rates for the 5 h reaction were determined and were related to the respective amounts of surface gold atoms ($GSNA_{ave}$). In xylene solution in the absence of K_2CO_3 , the activities of catalysts were characterized with 0–0.06 and 0–1.56 s^{-1} , $GSNA_{ini}$ and $ASNA_{ini}$ respectively. The catalysts deactivated below 10% conversion. The addition of K_2CO_3 resulted in a significant activity increase as reflected by 0.28–1.22 and 2.41–40.8 s^{-1} $GSNA_{ini}$ and $ASNA_{ini}$ values. The BzO selectivity was above 75% at around 70% conversion. The observed order of $GSNA_{ini}$ values under base free conditions is Au/SiO_2 (≈ 0) < Au/HAP < Au/Al_2O_3 < Au/MgO < $Au/MgAl_2O_4$, and in presence of K_2CO_3 is Au/SiO_2 < Au/Al_2O_3 < Au/HAP < $Au/MgAl_2O_4$ < Au/MgO . In the solvent-free experiments performed at 150 °C only the less exact average $GSNA_{ave}$ values after 5 h reaction were determined, which ranged between 0.16 and 0.83 s^{-1} (Au/Al_2O_3 < $Au/MgAl_2O_4$ < Au/HAP < Au/MgO < Au/SiO_2), however quite high conversions, > 85% (with the exception of Au/Al_2O_3 , 47%) were reached. The selectivities of the various samples are very different.

As demonstrated, for the interpretation of the obtained data the roles of active sites on gold nanoparticles of various dispersion, accessibility of the gold surface and the differing surface partial charge on gold, as well as the acid–base properties of various supports should be considered simultaneously in various extents depending the reaction conditions applied. Promoting role of water formed in the reaction with generation of surface hydroxyl groups is probably also important.

Acknowledgements Open access funding provided by MTA Wigner Research Centre for Physics (MTA Wigner FK, MTA EK). The authors are thankful to Ágnes Szegedi for the determination of the specific surface area of the HAP support. The financial support obtained for the Hungarian–Chinese bilateral cooperation in Project TET_15-1-2016-0120 is thankfully acknowledged.

Open Access This article is distributed under the terms of the Creative Commons Attribution 4.0 International License (<http://creativecommons.org/licenses/by/4.0/>), which permits unrestricted use, distribution, and reproduction in any medium, provided you give appropriate credit to the original author(s) and the source, provide a link to the Creative Commons license, and indicate if changes were made.

References

1. Ma Z, Dai S (eds) (2014) Heterogeneous gold catalysts and catalysis. RSC catalysis series. 592 pp
2. Haruta M (2011) Spiers memorial lecture: role of perimeter interfaces in catalysis by gold nanoparticles. *Faraday Discuss* 152:11–32
3. Abad A, Corma A, Garcia H (2008) Catalyst parameters determining activity and selectivity of supported gold nanoparticles for the aerobic oxidation of alcohols: the molecular reaction mechanism. *Chem Eur J* 14:212–222

- Ferraz CP, Garcia MAS, Teixeira-Neto É, Rossi LM (2016) Oxidation of benzyl alcohol catalysed by gold nanoparticles under alkaline conditions: weak vs. strong bases. *RSC Adv* 6:25279
- Kumar R, Gravel E, Hagège A, Li H, Jawale DV, Verma D, Namboothiri INN, Doris E (2013) Carbon nanotube-gold nanohybrids for selective catalytic oxidation of alcohols. *Nanoscale* 5:6491
- Castro KPR, Garcia MA, de Abreu WC, de Sousa SAA, de Moura CVR, Costa JCS, de Moura EM (2018) Aerobic oxidation of benzyl alcohol on a strontium-based gold material: remarkable intrinsic basicity and reusable catalyst. *Catalysts* 8:83
- Skupien E, Berger RJ, Santos VP, Gascon J, Makkee M, Kreutzer MT, Kooyman PJ, Moulijn JA, Kapteijn F (2014) Inhibition of a gold-based catalyst in benzyl alcohol oxidation: understanding and remediation. *Catalysts* 4:89–115
- Malláth T, Baiker A (2004) Oxidation of alcohols with molecular oxygen on solid catalysts. *Chem Rev* 104:3037–3058
- Fang W, Chen J, Zhang Q, Deng W, Wang Y (2011) Hydrothermalite-supported gold catalyst for the oxidant-free dehydrogenation of benzyl alcohol: studies on support and gold size effects. *Chem Eur J* 17:1247–1256
- Zope BN, Hibbitts DD, Neurock M, Davis RJ (2010) Reactivity of the gold/water interface during selective oxidation catalysis. *Science* 330:74–78
- Sankar M, Nowicka E, Tiruvalam R, He Q, Taylor SH, Kiely CJ, Bethell D, Knight DW, Hutchings GJ (2011) Controlling the duality of the mechanism in liquid-phase oxidation of benzyl alcohol catalysed by supported Au–Pd nanoparticles. *Chem Eur J* 17:6524–6532
- Feng J, Ma C, Miedziak PJ, Edwards JK, Brett GL, Li D, Du Y, Morgan DJ, Hutchings GJ (2013) Au–Pd nanoalloys supported on Mg–Al mixed metal oxides as multifunctional catalyst for solvent-free oxidation of benzyl alcohol. *Dalton Trans* 42:14498
- Galvanin F, Sankar M, Cattaneo S, Bethell D, Dua V, Hutchings GJ, Gavriilidis A (2018) On the development of kinetic models for solvent-free benzyl alcohol oxidation over a gold-palladium catalyst. *Chem Eng J* 342:196–210
- Boronat M, Corma A, Illas F, Radilla J, Ródenas T, Sabater MJ (2011) Mechanism of selective alcohol oxidation to aldehydes on gold catalysts: influence of surface roughness on reactivity. *J Catal* 278:50–58
- Tsunoyama H, Sakurai H, Tsukuda T (2006) Size effects on the catalysis of gold clusters dispersed in water for aerobic oxidation of alcohol. *Chem Phys Lett* 429:528–532
- Kozuch S, Martin ML (2012) “Turning over” definitions in catalytic cycles. *ACS Catal* 2:2787–2794
- Bligaard T, Bullock RM, Campbell CT, Chen JG, Gates BC, Gorte RJ, Jones CW, Jones WD, Kitchin JR, Scott SL (2016) Toward benchmarking in catalysis science: best practices, challenges and opportunities. *ACS Catal* 6:2590–2602
- Lente G (2013) Comment on “Turning over definitions in catalytic cycles”. *ACS Catal* 3:381–382
- Haider P, Kimmeler B, Krumeich F, Kleist W, Grunwaldt J-D, Baiker A (2008) Gold-catalyzed aerobic oxidation of benzyl alcohol: effect of gold particle size on activity and selectivity in different solvents. *Catal Lett* 125:169–176
- Guan Y, Hensen EJM (2009) Ethanol dehydrogenation by gold catalysts: the effect of the gold particle size and the presence of oxygen. *Appl Catal A* 361:49–56
- Centeno MA, Hadjiivanov K, Tz Venkov, Hr Klimev, Odriozola JA (2006) Comparative study of Au/Al₂O₃ and Au/CeO₂-Al₂O₃ catalysts. *J Mol Catal A* 252:142–149
- Kennedy D, Tezel FH (2014) Improved method for determining binary adsorption isotherms by using concentration pulse chromatography: adsorption of CO₂ and N₂ by silicalite at different pressures. *Adsorption* 20:189–199
- Shirani B, Eic M (2017) Novel differential column method for measuring multicomponent gas adsorption isotherms in NaY zeolite. *Ind Eng Chem Res* 56:1008–1018
- Nagy G, Benkó T, Borkó L, Csay T, Horváth A, Frey K, Beck A (2015) Bimetallic Au–Ag/SiO₂ catalysts: comparison in glucose, benzyl alcohol and CO oxidation reactions. *Reac Kinet Mech Cat* 115:45–65
- Li W, Wang A, Liu X, Zhang T (2012) Silica-supported Au–Cu alloy nanoparticles as an efficient catalyst for selective oxidation of alcohols. *Appl Catal A* 433–434:146–151
- Rodríguez-Reyes JCF, Friend CM, Madix RJ (2012) Origin of the selectivity in the gold-mediated oxidation of benzyl alcohol. *Surf Sci* 606:1129–1134
- Berndt H, Pitsch I, Evert S, Struve K, Pohl M-M, Radnik J, Martin A (2003) Oxygen adsorption on Au/Al₂O₃ catalysts and relation to the catalytic oxidation of ethylene glycol to glycolic acid. *Appl Catal A* 244:169–179

28. Choudhary VR, Dumbre DK (2011) Solvent-free oxidation of primary alcohols-to-aldehydes and aldehydes-to-carboxylic acids by molecular oxygen over MgO supported nano-gold catalyst. *Catal Commun* 13:82–86
29. Mitsudome T, Noujima A, Mizugaki T, Jitsukawa K, Kaneda K (2009) Efficient aerobic oxidation of alcohols using a hydrotalcite-supported gold nanoparticle catalyst. *Adv Synth Catal* 351:1890–1896
30. Choudhary VR, Dumbre DK (2009) Supported nano-gold catalysts for epoxidation of styrene and oxidation of benzyl alcohol to benzaldehyde. *Top Catal* 52:1677–1687
31. Li T, Liu F, Tang Y, Li L, Miao S, Su Y, Zhang J, Huang J, Sun H, Haruta M, Wang A, Qiao B, Li J, Zhang T (2018) Maximizing interfacial sites by single atom catalyst for solvent-free selective oxidation of primary alcohol. *Angew Chem Int Ed* 57:7795–7799
32. Abad A, Concepción P, Corma A, Garcia H (2005) A collaborative effect between gold and support induces the selective oxidation of alcohols. *Angew Chem Int Ed* 44:4066–4069
33. Li G, Enache DI, Edwards J, Carley AF, Knight DW, Hutchings GJ (2006) Solvent-free oxidation of benzyl alcohol with oxygen using zeolite-supported Au and Au–Pd catalysts. *Catal Lett* 110:7–13
34. Fu X, Ding Z, Zhang X, Weng W, Xu Y, Liao J, Xie Z (2014) Preparation of halloysite nanotube-supported gold nanocomposite for solvent-free oxidation of benzyl alcohol. *Nanos Res Lett* 9:282
35. Villa A, Gaiassi A, Rossetti I, Bianchi CL, van Benthem K, Veith GM, Prati L (2010) Au on MgAl₂O₄ spinels: the effect of support surface properties in glycerol oxidation. *J Catal* 275:108–116
36. Tang H, Wei J, Liu F, Qiao B, Pan X, Li L, Liu J, Wang J, Zhang T (2015) Strong metal-support interactions between gold nanoparticles and nonoxides. *J Am Chem Soc* 138:56–59
37. Beck A, Horvath A, Stefler G, Katona R, Geszti O, Tolnai G, Liotta LF, Guzzi L (2008) Formation and structure of Au/TiO₂ and Au/CeO₂ in mesoporous SBA-15. *Catal Today* 139:180–187
38. Prati L, Villa A (2012) The art of manufacturing gold catalysts. *Catalysts* 2:24–37
39. Jouve A, Nagy G, Somodi F, Tiozzo C, Villa A, Balerna A, Beck A, Evangelisti C, Prati L (2018) Gold–silver catalysts: effect of catalyst structure on the selectivity of glycerol oxidation. *J Catal* 368:324–335
40. Zhong C, Guo X, Mao D, Wang S, Wu G, Lu G (2015) Effects of alkaline-earth oxides on the performance of a CuO–ZrO₂ catalyst for methanol synthesis via CO₂ hydrogenation. *RSC Adv* 5:52958
41. Diez VK, Apesteguia CR, Di Cosimo JI (2000) Acid–base properties and active site requirements for elimination reactions on alkali-promoted MgO catalysts. *Catal Today* 63:53–62
42. Pan Z, Zhao CY (2015) Dehydration/hydration of MgO/H₂O chemical thermal storage system. *Energy* 82:611–618
43. Anderson JR (1975) *Structure of metallic catalysts*. Academic Press, Cambridge
44. Li H, Li L, Pedersen A, Gao Y, Khetrpal N, Jónsson H, Zeng XC (2015) Magic-number gold nanoclusters with diameters from 1 to 3.5 nm: relative stability and catalytic activity for CO oxidation. *Nano Lett* 15:682–688
45. Hadjiivanov KI, Vayssilov GN (2002) Characterization of oxide surfaces and zeolites by carbon monoxide as an IR probe molecule. *Adv Catal* 47:307–511
46. Hr Klimev, Fajerweg K, Chakarova K, Delannoy L, Louis C, Hadjiivanov K (2007) Oxidation of gold metal particles supported on TiO₂: an FTIR study by means of low-temperature CO adsorption. *J Mater Sci* 42:3299–3306
47. Yang K, Liu J, Si R, Chen X, Dai W, Fu X (2014) Comparative study of Au/TiO₂ and Au/Al₂O₃ for oxidizing CO in the presence of H₂ under visible light irradiation. *J Catal* 317:229–239
48. Haider P, Urakawa A, Schmidt E, Baiker A (2009) Selective blocking of active sites on supported gold catalysts by adsorbed thiols and its effect on the catalytic behavior: a combined experimental and theoretical study. *J Mol Catal A* 305:161–169
49. Enache DI, Knight DW, Hutchings GJ (2005) Solvent-free oxidation of primary alcohols to aldehydes using supported gold catalysts. *Catal Lett* 103:43–52
50. Choudhary VR, Dhar A, Jana P, Jha R, Uphade BS (2005) A green process for chlorine-free benzaldehyde from the solvent-free oxidation of benzyl alcohol with molecular oxygen over a supported nano-size gold catalyst. *Green Chem* 7:768–770

51. Kokate M, Dapurkar S, Garadkar K, Gole A (2015) Magnetite–silica–gold nanocomposite: one-pot single-step synthesis and its application for solvent-free oxidation of benzyl alcohol. *J Phys Chem C* 119:14214–14223

Publisher's Note Springer Nature remains neutral with regard to jurisdictional claims in published maps and institutional affiliations.

Affiliations

Gergely Nagy¹ · Andrea Beck¹ · György Sáfrán² · Zoltán Schay¹ · Shaofeng Liu^{3,4} · Tianbo Li³ · Botao Qiao³ · Junhu Wang^{3,4} · Károly Lázár⁵

✉ Károly Lázár
lazar.karoly@energia.mta.hu

¹ Department of Surface Chemistry and Catalysis, Centre for Energy Research, HAS, Konkoly Thege M. út 29-33, Budapest 1121, Hungary

² Laboratory of Thin Layer Physics, Institute of Materials Science, Centre for Energy Research, HAS, Konkoly Thege M. út 29-33, Budapest 1121, Hungary

³ State Key Laboratory of Catalysis, Dalian Institute of Chemical Physics, Chinese Academy of Sciences, 457 Zhongshan Road, Dalian 116023, China

⁴ Mössbauer Effect Data Center, Dalian Institute of Chemical Physics, Chinese Academy of Sciences, 457 Zhongshan Road, Dalian 116023, China

⁵ Department of Nuclear Analysis and Radiography, Centre for Energy Research, HAS, Konkoly Thege M. út 29-33, Budapest 1121, Hungary